Journal Pre-proof

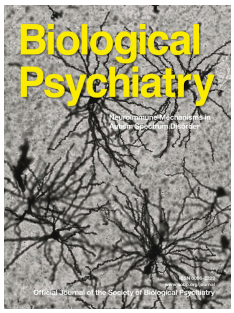

Dynamics of cortical degeneration over a decade in Huntington's disease

Eileanoir B. Johnson, Gabriel Ziegler, William Penny, Geraint Rees, Sarah J. Tabrizi, Rachael I. Scahill, Sarah Gregory

PII: S0006-3223(20)32069-2

DOI: https://doi.org/10.1016/j.biopsych.2020.11.009

Reference: BPS 14382

To appear in: *Biological Psychiatry*

Received Date: 6 March 2020

Revised Date: 14 October 2020

Accepted Date: 8 November 2020

Please cite this article as: Johnson E.B., Ziegler G., Penny W., Rees G., Tabrizi S.J., Scahill R.I. & Gregory S., Dynamics of cortical degeneration over a decade in Huntington's disease, *Biological Psychiatry* (2020), doi: https://doi.org/10.1016/j.biopsych.2020.11.009.

Dynamics of cortical degeneration over a decade in Huntington's disease

Eileanoir B. Johnson[1,*], Gabriel Ziegler[2,3,*], William Penny[4], Geraint Rees[5], Sarah J. Tabrizi[1], Rachael I. Scahill[1], Sarah Gregory[1]

[1] Department of Neurodegenerative Disease, UCL Queen Square Institute of Neurology, University College London, London WC1N 3BG, United Kingdom

[2] Institute of Cognitive Neurology and Dementia Research, Otto-von-Guericke-University Magdeburg, 39120 Magdeburg, Germany

[3] German Center for Neurodegenerative Diseases (DZNE), 39120 Magdeburg, Germany

[4] School of Psychology, University of East Anglia, Norwich NR4 7TJ, United Kingdom

[5] Wellcome Centre for Human Neuroimaging, UCL Queen Square Institute of Neurology, University College London, London WC1N 3BG, United Kingdom

* These authors contributed equally to this work

Correspondence

Eileanoir B. Johnson
Huntington's Disease Centre
UCL Queen Square Institute of Neurology
University College London
United Kingdom
Phone: +44 203 108 7476
Email: eileanoir.johnson@ucl.ac.uk

Gabriel Ziegler
Institute of Cognitive Neurology and Dementia Research
Otto-von-Guericke-University Magdeburg
Leipziger Str. 44
39120 Magdeburg
Germany
Phone: +49 / 391 67 250 54
Email: gabriel.ziegler@dzne.de

Running title: Mapping cortical degeneration in Huntington's disease

Keywords: Imaging; Longitudinal; Huntington's disease; Atrophy; Cortex; Subcortex.

Abstract

Background

Characterizing changing brain structure in neurodegeneration is fundamental to understanding long-term effects of pathology and ultimately providing therapeutic targets. It is well-established that Huntington's disease (HD) gene-carriers undergo progressive brain changes during the course of disease, yet the long-term trajectory of cortical atrophy is not well-defined. Given that genetic therapies currently tested in HD are primarily expected to target the cortex, understanding atrophy across this region is essential.

Methods

Capitalizing on a unique longitudinal dataset with a minimum of three and maximum of seven brain scans from 49 HD gene-carriers and 49 age-matched controls, we implemented a novel dynamical systems approach to infer patterns of regional neurodegeneration over ten years. We use Bayesian hierarchical modelling to map participant- and group-level trajectories of atrophy spatially and temporally, additionally relating atrophy to the genetic marker of HD (CAG-repeat length) and motor and cognitive symptoms.

Results

We show, for the first time, that neurodegenerative changes exhibit complex temporal dynamics with substantial regional variation around the point of clinical diagnosis. Although widespread group differences were seen across the cortex, occipital and parietal regions undergo the greatest rate of cortical atrophy. We have established links between atrophy and genetic markers of HD, while demonstrating that specific cortical changes predict decline in motor and cognitive performance.

Conclusions

HD gene-carriers display regional variability in the spatial pattern of cortical atrophy, which relates to genetic factors and motor and cognitive symptoms. Our findings indicate a complex pattern of neuronal loss, which enables greater characterization of HD progression.

Introduction

Characterizing the temporal trajectory of cortical atrophy is important for the development of mechanistic theories of neurodegeneration. Uncovering cortical areas that undergo atrophy along with associated atrophy rates during different phases of neurodegeneration can provide insights into the biological underpinnings of neurodegenerative disease. Until now, characterizing dynamic patterns of brain change has been limited by the lack of suitable modelling frameworks and cohort data with extensive timepoints (1), resulting in limited knowledge of the nature of long-term brain changes. Here, we use a Huntington's disease (HD) cohort to validate a novel method of quantifying longitudinal trajectories of neurodegeneration over a large number of timepoints. HD is an ideal neurodegenerative condition in which to validate this technique due to a definitive genetic test long before symptom onset and clinical diagnosis, and it is a well-phenotyped progressive neurodegenerative disease (2).

Despite detailed knowledge of the genetic cause and symptoms of HD, the underlying cellular mechanisms and pathophysiology are not well-understood. There is robust evidence that striatal degeneration begins over a decade before symptom onset (3,4) and continues at a constant rate (5–9). By early manifest disease cortical atrophy appears to have occurred (4), but the ongoing *process* of grey matter (GM) degeneration in HD has not been studied. There is evidence of increasing white matter (WM) disorganization during this period (10–13), but conflicting findings regarding the cortex, with regional cortical change only described between two timepoints over short intervals and via restrictive analysis techniques (6,14–19), such as regression models. As HD is a slowly progressive disease, these studies ultimately fail to capture the nature or extent of cortical change. It has proven challenging to understand the neural bases

of heterogeneity in HD onset and symptom progression, despite an apparent association between postmortem cortical degeneration and symptomatology prior to death (20). With the advent of genetic therapies targeting the cortex (21), understanding long-term cortical processes and their impact on clinical progression is essential.

Here, we apply a novel modelling technique to map volumetric brain changes and associated clinical changes over 10 years in a large group of HD gene-carriers. This technique, which capitalizes on Bayesian hierarchical modelling, offers a powerful approach to defining change across numerous data points. Furthermore, it can be used to test for causal interactions between changes in different brain regions. The approach constructs individual participant-level dynamic models of atrophy, which are used to identify group-wise trajectories of disease progression both spatially and temporally (22). By specifying temporal progression of cortical atrophy within all brain regions simultaneously (23) both total atrophy and, uniquely, rates of atrophy over multiple time points can be understood. These new insights reveal not only where change occurs but, for the first time, how the pace of regional neurodegeneration varies across the cortex. Importantly, the model can examine the influence of external factors on brain changes (e.g. genetic components), causal patterns of inter-regional interactions, and predict behavioural scores from regional atrophy. We apply this technique (22–24) to compare cortical brain changes in a cohort of HD gene-carriers undergoing motor onset during a ten year period with an age-matched control group from the multisite, longitudinal TRACK-HD and TrackOn-HD studies (4,6,7,14,25). Motor onset is a critical period in HD progression and is used as a proxy for diagnostic disease onset. During this period, increasing prevalence of motor symptoms results in increased clinical intervention and greater disruption to everyday functioning and mental

wellbeing (26). The nature of motor symptoms suggests a breakdown of the motor network, but to understand the progression in motor symptoms, long-term mapping of degeneration trajectories alongside clinical measures is essential.

We analyzed up to seven individual annual MRI scans per participant, plus motor and cognitive performance for the HD group, focusing on volumetric measures from widespread cortical (and subcortical) brain regions using a protocol optimized for this cohort (27). We investigated in which regions HD patients show lower volume at point of diagnosis, and how rates of atrophy vary across the cortex during this period compared to controls. We predicted that subcortical atrophy would show the greatest degeneration (28), with regions of the frontal, parietal and occipital cortex also expected to show atrophy. We hypothesized that participants with higher CAG-repeat lengths (the genetic cause of HD) would undergo greater atrophy.

Methods and materials

Participants

Participants were from the TRACK-HD and TrackOn-HD cohorts (4,25). PreHD participants from both cohorts who subsequently transitioned to manifest HD ('converters') during data collection were included and used to create a group experiencing a similar stage of disease progression. Control participants were selected from the same datasets to match the HD group as closely as possible for age, sex, site and number of visits (Supplementary Methods). The study was approved by the local ethics committees, and written informed consent was obtained from each participant according to the Declaration of Helsinki.

To increase homogeneity of disease progression and define a comparable progression time variable, data were re-aligned to consolidate year of motor conversion across all participants (Supplementary Fig. 1). The first year of Diagnostic Confidence Score=4 was designated as year of conversion (timepoint=0), and each year prior to conversion labelled as year -1, -2, -3, etc. Every year after conversion was labelled as year 1, 2, 3, etc. Individual variability of changes beyond the synchronizing event of motor diagnosis was accounted for during modelling. Every HD participant was matched to a control participant, who were aligned with 'timepoint 0' the point at which age matched their corresponding HD participant. Participants had a minimum of three and maximum of seven timepoints (HD mean: 5.84 scans, SD: 1.63; Control mean: 6.06 scans, SD: 1.45).

The Unified Huntington's Disease Rating Scale Total Motor Score (TMS) was used to approximate clinical motor progression (29) (Supplementary Methods). The Symbol Digit Modalities Test (SDMT) was included as a measure of cognitive progression (30). SDMT is a cognitive task designed to measure visual processing and psychomotor speed, established as the most reliable and sensitive cognitive measure for detecting change in premanifest and manifest HD (31,32), and related to HD progression (7). Both scores were (inverted and) rescaled to [0,100] to the min/max observation in the HD sample with an increase indicating worsening symptoms.

MRI data acquisition

T1-weighted scans were acquired from four 3Tesla scanners with acquisition protocols the same for both studies (Supplementary Methods).

Longitudinal image processing

A longitudinal within-participant registration pipeline from SPM12 was used to create an average image for each participant (33); this was parcellated into 138 regions using MALP-EM, a fully automated segmentation tool (34) validated for use in HD (27). Each average segmented region was multiplied by Jacobian deformation maps (derived from registration) to create a volumetric map for each region for each timepoint (see Supplementary Methods). All segmentations underwent visual QC. One dataset failed QC due to segmentation errors.

To reduce noise within small cortical regions, segmentations were combined into 55 larger regions based on spatial localization and visual inspection (Supplementary Table 1). 50 cortical regions (25 bilateral pairs), four subcortical regions (bilateral caudate and putamen) and one global WM region were included. To facilitate clear across-region comparisons, regional brain volumes (%) relative to sample overall mean volume at timepoint of motor diagnosis (set to 100%) were analyzed.

Hierarchical disease progression model using Bayesian inference

Hierarchical (multilevel) modelling is an increasingly popular approach for modelling longitudinal data, outperforming classical regression in predictive accuracy (35). Here we used a previously established framework for dynamic modelling of longitudinal structural MRI (23) using Bayesian inference (22), Fig. 1. We summarize relevant components of the model here (and Supplementary Methods) and refer the mathematically-interested reader to a more technical

introduction (23,36,37). The dynamical system used for modelling brain changes is generally described via state model

$$\frac{dx}{dt}(t) = Ax(t) + Cu(t, \theta_u)$$

and observational (or measurement) model

$$y(t) = g\big(x(t), \theta_g\big) + \epsilon$$

with multivariate observations $y(t)$, state variables $x(t)$, system inputs $u(t,.)$, connectivity parameter matrix A, regional sensitivity parameter to inputs C, and residuals ϵ. More specifically, the state equation models temporal progression of the state vector *x(t)*, referring to 27 bilateral volumes (25 cortical regions, caudate and putamen) and one global WM volume over 10 year periods (t= -6, …, 5 years relative to diagnosis).

The progression of states is influenced by both, endogenous dynamics $Ax(t)$, and external time-varying inputs $u(t, \theta_u)$ with optional input parameters θ_u. The endogenous dynamics of the HD model were restricted to regional self-connections, which can be interpreted as region-specific atrophy (or decay) rates resulting in approximately linear volume loss over the course of progression. We assumed bilateral symmetry of disease progression across hemispheres and thus the same state variable describes evolution of volumes in both corresponding bilateral GM ROIs (via a linear observational model g that averages both hemispheres). In summary, the generative model makes predictions for 55 brain regions using 28 dynamical state variables describing region-specific volume progression during the decade around disease onset. Three to seven available scans per person were used to optimize both individual- and group-level model parameters in a two-stage procedure.

As outlined in Zeidman et al. (36,37) the Bayesian modelling framework enables comparison of alternative individual-and group-level models that implement hypotheses about brain data. However, since our goal was regional mapping of *a-priori* unknown structural disease progression dynamics, we applied this approach in a more exploratory way. We compared four conventional and novel individual (first)-level state models that might be useful to describe volume progression towards HD (Fig.1B): (a) linear model i.e. constant rate of atrophy ($A=0$, $C\neq0$, $u(t)=c_0$); (b) quadratic model i.e. accelerated change ($A=0$, $C\neq0$, $u(t)=c_0+c_1t$); (c) a simple dynamic model without inputs (i.e. $A\neq0$, $C=0$); (d) a more complex dynamic model with sigmoidal input u (Supplementary Methods). The choice of a sigmoidal input was motivated by its wide use in the context of hypothetical and data-driven models of other neurodegenerative diseases (38–41). Each of these first-level models (a-d) were estimated for each participant and inverted using Variational Laplace methods (24).

Multilevel modelling increases power for detecting group-level effects by modelling differences and uncertainty in first-level parameters, while accounting for differing number of visits. First-level models for each participant were embedded in a second-level model to estimate group-wise brain change, the advantages of which are discussed in Supplementary Methods, but pertain to statistical efficiency and mitigating risk of overfitting. Bayesian hierarchical models for each of the four first-level models (a-d) were estimated using Parametric Empirical Bayes (PEB) (22,36), incorporating a second-level design matrix with overall sample mean, diagnostic group difference and covariates including CAG-repeat length, sex, age (at motor diagnosis), total intracranial volume and site (age orthogonalized w.r.t CAG due to high correlation).

Bayesian Model Selection (BMS) was then used to compare statistical evidence for each of the above models (a-d) at the whole-sample level. BMS optimizes model fit while penalizing complexity and is appropriate for use in highly parameterized hierarchical disease progression models (42). Of the four models, evidence was highest for the simple dynamic model (state equation $dx/dt=Ax$) using no inputs (Fig. 1C). Consequently, the optimal model was found to be comparably parsimonious. Notably, we follow recommendations from the American Statistical Association (43) and use Bayesian inference in our main analysis (Supplementary Methods), although some p-value hypothesis tests are reported for demographics. For all group-level model parameters, such as group difference of the initial state (volume at diagnosis) or (log) decay rate, we present (Bayesian) posteriors mean ± SD. Moreover, as suggested by Zeidman et al. (36) we used Bayesian Model Reduction and averaging (BMA) to reduce numbers of parameters and threshold parameters of winning model based on Free Energy. This involved, for each second level parameter j, performing a Bayesian model comparison of the hierarchical PEB model with parameter j 'switched on' (free to vary) versus the equivalent PEB model with parameter j 'switched off' (fixed at its prior expectation of zero). Difference in evidence can then be converted to a posterior probability. Results focus on parameters from the BMA that exceed the posterior probability threshold of 0.95.

Next, we extended the observational model to investigate possible inter-regional dynamics of morphometry during HD progression, and additionally predict motor and cognitive symptom scores (Supplementary Methods). For further validation of the hierarchical dynamical model we assessed its predictive validity to determine clinical significance of model parameters using

leave-one-out cross-validation. The above winning model was fitted to all but one participant, and covariates (group membership HD vs. NO and CAG) for the left-out participant predicted. This was repeated with each participant left out and accuracy of the prediction recorded (Supplementary Fig. 2). Predictive validity when using model parameters to predict individual group membership was found to be very high with 97 of 98 subjects correctly assigned using their posterior probabilities (estimated and true group variable correlate r=0.9). When predicting CAG, estimated and true values correlated r=.41.

Data and code availability

Requests for access to TRACK-HD and TrackOn-HD data should be made via the CHDI Foundation. Links to custom-made scripts and synthetic example dataset demonstrating dynamic modelling of longitudinal HD data can be provided upon request to corresponding authors (Supplementary Methods).

Results

Sample

We analyzed longitudinal data from 49 HD gene-carriers with three to seven individual annual scans (mean: 5.84 SD: 1.63) over a follow-up time of two to six years (mean: 5.94 SD: 1.62), and 49 control participants with three to seven annual scans (mean: 6.08, SD: 1.45; Supplementary Fig. 1). 30 HD participants and 33 control participants had seven annual scans. Demographics are shown in Table 1. There was no significant group difference in age. As expected, HD gene-carriers with longer CAG-repeat length had earlier clinical diagnosis (r=-0.85, p<e-13).

Widespread group differences at HD motor diagnosis

When comparing HD participants to age-matched control participants at timepoint of motor diagnosis, there were widespread differences in volume across the brain. As predicted, caudate and putamen showed the largest differences (Figure 2), with regions across all lobes also showing group differences, demonstrating that cortical atrophy is extensive even at this early stage of HD.

Atrophy over a decade is variable across the cortex

Over a decade of HD progression, when compared to controls, the highest total volume reduction was in striatal regions; the putamen and caudate showing 18.7% and 15.4% loss of baseline volume in HD, but less than 3% for both regions in controls (Fig. 3A). The rate of volume loss was higher in widespread cortical areas for HD participants (Figure 3B, Supplementary Fig. 3), particularly occipital and parietal regions (superior parietal lobule, precentral gyrus). These findings highlight pronounced posterior atrophy during the long-term transition from preHD to manifest HD, suggesting a distinct spatio-temporal pattern of change associated with clinical presentation.

Brain atrophy is related to genetic burden in some regions

We further analyzed the link between CAG-repeat length and atrophy across brain regions. CAG-repeat length predicted rate of atrophy in occipital, parietal- and striatal regions (Fig. 4A), suggesting greater vulnerability of the occipital lobe in particular to increased genetic burden.

Moreover, systematic effects of CAG-repeat length on progression were reflected in the increasing variance of atrophy explained by gene differences (Fig. 4B).

No evidence for inter-regional progression

To explore potential disease spread within the cortex, we compared models that enabled associations of atrophy dynamics between subcortical-cortical and cortical-cortical regions. More specifically, we included between-region connections to test whether atrophy state in one brain area caused volume change in another (connected) brain area. However, model comparisons revealed highest evidence for models without inter-regional interactions (Supplementary Fig. 4 and Methods), suggesting that either the pattern of regional atrophy is better described independently or that the spread of atrophy during HD progression follows a more complex pattern.

Cortical atrophy can be tied to individual motor and cognitive symptom changes

Finally, to evaluate how regional brain atrophy might contribute to emerging motor and cognitive symptoms, we extended our HD progression model to a longitudinal brain-behavioral framework (Supplementary Fig. 5A & 6, and Methods) including (1) brain volumes; (2) TMS motor assessments (44); and (3) cognitive symptoms using SDMT (30) in HD participants only. Over a decade, TMS performance was reduced by 57.80%, and SDMT by 16.78%, and the determination coefficient R^2 was 0.82 for TMS and 0.89 for SDMT suggesting a strong model fit. In predicting individual TMS changes, atrophy in a number of regions contributed to worsening TMS; the entorhinal area, cingulate, parahippocampal gyrus, caudate, calcarine

cortex, supplementary motor cortex, temporal pole, frontal gyrus, lingual gyrus, cuneus and planum temporale were all predictors of worsening TMS (Fig. 5A, Supplementary Fig. 6). When using the model to predict change in SDMT, we found a pattern suggesting that the difference between cortical and striatal atrophy was predictive of cognitive worsening (Fig. 5B). That is, in participants undergoing similar rates of putamen atrophy, those with particularly emphasized cortical atrophy in the cingulate, orbital gyrus, occipital gyrus, lingual gyrus and entorhinal area experienced greater cognitive decline.

Discussion

HD is a devastating neurological condition with a complex interplay of physiological, neuronal and behavioral changes (2). This study provides a novel characterization of long-term cortical atrophy during a critical period in HD progression - onset of motor symptoms. Although previous studies suggest that pathological changes occur cortically (4,17,45,46), they give little insight regarding long-term trajectories and association with worsening symptomatology. Heterogeneity of cognitive and psychiatric symptoms many years prior to motor decline (47) suggests individual variability in pathology-related brain changes. Using a Bayesian dynamic modelling framework applied to a large multi-site longitudinal sample of participants at the same disease stage, we have shown widespread cortical volume differences across the cortex in HD participants during motor diagnosis when compared to controls. Interestingly, our results indicate that in the period surrounding motor diagnosis the trajectory of volumetric change is variable across the cortical mantle, with highest rates of cortical atrophy in occipital regions.

There were differences between gene-carriers at motor diagnosis and controls across the cortex; with occipital, frontal temporal and parietal areas showing lower volume in HD. The occipital lobe showed fastest rates of atrophy, with parietal regions also showing significantly greater change. In contrast, rates of changes in anterior and temporal regions showed smaller differences. In terms of clinical and behavioral markers, CAG-repeat length, the key marker of genetic burden and individual disease onset (2), was most predictive of individual rate of volume decline within occipital regions. The entorhinal area, cingulate, and regions of the occipital, frontal and temporal lobes were associated with worsening motor performance, where cognitive decline was associated with atrophy in occipital, cingulate and lingual regions. Our framework models regional brain alterations in relation to behavior and clinical changes, rather than simply correlating cortical atrophy with symptoms across participants (17,48) and we present the first detailed picture of the process of cortical changes during disease onset and their direct effect on symptoms.

Although HD participants showed significantly lower volumes in frontal and temporal regions compared to controls, these anterior regions did not show significantly greater rates of atrophy, suggesting that anterior atrophy occurs earlier in the disease course. Cognitive and psychiatric symptoms typically become apparent prior to motor symptoms, and studying participants further from onset would explore the link between earlier emergence of these symptoms and fronto-temporal atrophy.

Interestingly, during motor onset cortical atrophy appears to contribute more to cognitive decline than that of the striatum. SDMT, measuring psychomotor speed and visual processing, recruits

widespread areas of fronto-parietal and fronto-occipital networks along with tempo-parietal and inferior frontal cortices (49). We observed an association between SDMT performance and atrophy progression in occipital regions, along with the cingulate and lingual gyrus, regions recruited during SDMT performance (50). Our results suggest that in participants showing similar rates of striatal atrophy, those with greater cortical atrophy in these regions might also undergo greater decline in SDMT performance. As such, cortical rather than striatal atrophy appears to be predictive of individual cognitive decline, with higher between-participant variability possibly due to unknown mediating factors resulting in partially independent progression trajectories of cortical and subcortical atrophy.

Conversely, we show that increased atrophy in a range of regions is associated with worsening motor scores. A number of regions, including the entorhinal area, cingulate, parahippocampal gyrus, caudate, calcarine cortex, supplementary motor cortex, lingual gyrus and cuneus are associated with spatial, motor and visual performance. Given that TMS assesses motor behavior, eye movement, and clinical characteristics of HD it is perhaps unsurprising that TMS is associated with cortical regions linked to a range of functions.

Using our Bayesian dynamic modelling framework, we also explored between-region ‘spreading’ of cortical atrophy, but found no evidence of between-region progression of atrophy. It is likely that inter-regional interactions between cortical areas follow more complex processes than simple striatal-cortical or cortical-cortical spread, with other tissue types and variable time-lag factors playing a role. The integration of diffusion metrics into the model could help elucidate these processes. Alternatively, more power may be required. Future work will evaluate

this theory by including multi-modal and micro-structural measures within the longitudinal modelling framework and investigate inter-region progression.

An additional strength of our approach is that it not only allows inference of group-level changes but examines contribution of genetic risk factors to individual differences in progression of atrophy. CAG-repeat length showed a positive relationship with increased atrophy in subcortical and occipital regions, supporting a potential link between higher CAG-repeat length and HD progression (7,51) particularly within subcortical and occipital regions (15,52,53). Previous work has also demonstrated substantial occipital lobe atrophy in both pre-HD and manifest-HD (4,6,15,54). The association between CAG-repeat length and occipital atrophy suggests that early visual regions are impacted by genetic burden more than other cortical regions, highlighting a differential relationship between cortical atrophy and genetic burden.

The ability of our modelling approach to detect subtle regional volume changes may make it an ideal model for analysis of clinical trial data in neurodegeneration. If a disease-modifying treatment were successful in changing the course of neurodegeneration, differences in neural atrophy between placebo and treatment groups could be anticipated. This model can be applied to any brain region and participant group, encouraging application of our model to all neurodegenerative conditions. In HD, for example the caudate, putamen or sensory-motor regions could be measured to track effects of disease-modifying treatments (dependent on the predicted treatment effects), whereas in frontotemporal dementia regions of the insula or temporal lobes could be selected instead (55).

The modelling framework used here was developed to address weaknesses in previous analysis methods and approach quantification of GM change via a dynamic systems method (23) in a unique longitudinal HD cohort. The ability to quantify changes in cortical GM atrophy over time, while accounting for individual variability over multiple timepoints offers a more powerful approach than previous methods of structural MRI modelling (56,57). Indeed, the results of our leave-one-out cross-validation analysis indicate that our model is appropriate for modelling our data. However, it is important to consider that the use of clinical-rated motor diagnosis for temporal alignment of the progression of all participants in our model introduces some potential between-participant error, since participants were seen yearly and could have converted at any point between two visits. Moreover, our focus on participants within six years of motor onset prevents us studying the very earliest cortical atrophy patterns. However, we carefully accounted for differences due to age, sex, total intracranial volume and site to render the group inference unbiased. The regional progression observed during a particularly crucial period in HD progression is, therefore, clinically meaningful, and supported by previous imaging data, indicating that the model successfully illustrates longitudinal neurodegeneration in unprecedented depth.

In conclusion, our findings provide the most detailed characterization of cortical atrophy in Huntington's disease presented to-date. By applying a recently validated model that is uniquely able to map temporal and spatial cortical change within a genetically confirmed HD cohort, we have demonstrated that cortical atrophy shows regional variability related to genetic factors and predicts motor and cognitive performance, representing changes within the HD phenotype. This work represents a principled approach to modelling longitudinal structural MRI data that offers

new insights into the spatial and temporal phenotype of cortical changes, and in turn the biological underpinnings of neurodegeneration.

		HD	Controls
Age		44.59 (9.28) 28.65-66.00	44.51 (9.04) 28.85-66.06
Female		27 (55.10%)	30 (61%)
CAG		43.67 (2.77) 39.00-50.00	n/a
Site	**Leiden (21)**	22 (44.90%)	14 (28.57%)
	London (10)	10 (20.40%)	10 (20.40%)
	Paris (10)	10 (20.40%)	14 (28.57%)
	Vancouver (7)	7 (14.29%)	11 (22.45%)

Table 1. Demographics for the 49 participants included in this longitudinal multi-centre study. The table shows mean (SD) and range, or N (%).

Figure legends

Fig. 1. Model illustration and Bayesian model comparison. (A) An illustration of participant-level models. The model is defined by a system describing changes in observed volumes (squares) using 28 regional latent state variables (round circles) during the period studied. The states are negatively self-connected causing region-specific decline (atrophy) of volume. **(B)** Illustration of system inputs (red circle) that were explored cause different forms of acceleration of pathology during transition from pre-symptomatic to symptomatic disease phase. In case of presence of non-linearities, the rate of change (velocity) of progression might not be constant (top), but change linearly with progression time (middle), or transitions smoothly following a sigmoidal shape (bottom). **(C)** Approx. model evidence of multiple models compared. All models compared were hierarchical with subject- and a group-level describing commonalities and control/HD differences, covariates and confounds.

Fig. 2: Volume differences between HD and controls at point of motor diagnosis. Group differences of volumes (HD<NO) at timepoint of motor diagnosis as predicted by the dynamic disease progression model. Shown are surface projections (left) and bar plots ± SD (right panel) of the group level regional offset parameters (initial states) at timepoint zero obtained from Bayesian model reduction and averaging. White indicates non-significant group differences. Only significant regions shown in bar plot.

Fig. 3: Total brain atrophy during Huntington's disease motor conversion and rates of atrophy during Huntington's disease motor conversion. (A) Parameter plot of the overall percent volume loss per region per decade approximated by a linear model. Median total volume loss (in % per decade) are presented using a non-hierarchical model to minimize influence of priors on group and region-specific rates of change. However, results were coarsely consistent with predictions from dynamical Bayesian hierarchical further presented. **(B)** Significant rate of atrophy in group differences (HD>NO) over a decade around HD motor onset. Decay rate refers to self-connection parameters of regional volume states (see methods). Both panels use log scale for illustration. All results are group level estimates based on longitudinal dynamic modelling and account for effects of age, sex, CAG and confounds.

Fig. 4: CAG repeat length is related to rate of cortical and striatal atrophy. (A) A brain surface projection and **(B)** parameter ± SD that indicates whether individual CAG repeat length predicts regional rate of atrophy. Participants with higher CAG repeat length show increased rate of atrophy, especially in posterior cortical and striatal areas. White indicates non-significant CAG effects. Only significant regions shown in bar plot. Analysis from Bayesian model average accounting for effects of age, sex and confounds (see methods). (**B)** Proportion of total variance of volume in Caudate/Putamen/White matter explained (i.e. R^2) by CAG repeat length. We show R^2 over all timepoints 6 years before to 5 years after diagnosis. X-axis: disease progression time in years relative to individual motor diagnosis.

Fig. 5: Brain-behavioral model predicts symptom changes during transition to HD. (A) Surface projection of weights that indicate whether a brain region contributes to the prediction of longitudinal motor scores over all timepoints (for model illustration and details see Supplementary Fig. 5 and a bar plot of weights in Supplementary Fig. 5B and 5C). Results are from group-level model accounting for effects of age, sex, CAG and confounds (see methods). The right panels illustrates observed TMS scores (scaled to 0-100, gray) and individual model predictions (green) for 5 exemplary participants with varying CAG length, group level model predictions (blue) using our HD progression model (blue). See Supplementary Fig. 6 for all HD participant plots. X-axis: disease progression time in years relative to individual motor diagnosis. (B) Analogous findings for brain-based prediction of cognitive deficits (SDMT score, inverted and scaled 0-100, bar plot of weights in Supplementary Fig. 5).

References

1. Young AL, Oxtoby NP, Schott JM, Alexander DC (2014): Data-driven models of neurodegenerative disease. *Adv Clin Neurosci Rehabil* 14: 6–9.

2. Bates GP, Dorsey R, Gusella JF, Hayden MR, Kay C, Leavitt BR, *et al.* (2015): Huntington disease. *Nat Rev Dis Prim* 15005.

3. Vonsattel JP, Myers RH, Stevens TJ, Ferrante RJ, Bird ED, Richardson EP (1985): Neuropathological classification of Huntington's disease. *J Neuropathol Exp Neurol* 44: 559–77.

4. Tabrizi SJ, Langbehn DR, Leavitt BR, Roos RA, Durr A, Craufurd D, *et al.* (2009): Biological and clinical manifestations of Huntington's disease in the longitudinal TRACK-HD study: cross-sectional analysis of baseline data. *Lancet Neurol* 8: 791–801.

5. Rees E (2014): Development and evaluation of biomarkers in Huntington's Disease: furthering our understanding of the disease and preparing for clinical trials. *Dr thesis, UCL (University Coll London)* . Retrieved February 16, 2018, from http://discovery.ucl.ac.uk/1455986/

6. Tabrizi SJ, Scahill RI, Durr A, Roos RA, Leavitt BR, Jones R, *et al.* (2011): Biological and clinical changes in premanifest and early stage Huntington's disease in the TRACK-HD study: the 12-month longitudinal analysis. *Lancet Neurol* 10: 31–42.

7. Tabrizi SJ, Scahill RI, Owen G, Durr A, Leavitt BR, Roos RA, *et al.* (2013): Predictors of phenotypic progression and disease onset in premanifest and early-stage Huntington's disease in the TRACK-HD study: analysis of 36-month observational data. *Lancet Neurol*

12: 637–649.

8. Aylward EH, Sparks BF, Field KM, Yallapragada V, Shpritz BD, Rosenblatt A, *et al.* (2004): Onset and rate of striatal atrophy in preclinical Huntington disease. *Neurology* 63: 66–72.

9. Langbehn DR, Stout JC, Gregory S, Mills JA, Durr A, Leavitt BR, *et al.* (2019): Association of CAG Repeats with Long-term Progression in Huntington Disease. *JAMA Neurol*. https://doi.org/10.1001/jamaneurol.2019.2368

10. Zhang J, Gregory S, Scahill RI, Durr A, Thomas DL, Lehericy S, *et al.* (2018): In vivo characterization of white matter pathology in premanifest huntington's disease. *Ann Neurol*. https://doi.org/10.1002/ana.25309

11. McColgan P, Gregory S, Seunarine KK, Razi A, Papoutsi M, Johnson E, *et al.* (2017): Brain Regions Showing White Matter Loss in Huntington's Disease Are Enriched for Synaptic and Metabolic Genes. *Biol Psychiatry*. https://doi.org/10.1016/j.biopsych.2017.10.019

12. McColgan P, Seunarine KK, Razi A, Cole JH, Gregory S, Durr A, *et al.* (2015): Selective vulnerability of Rich Club brain regions is an organizational principle of structural connectivity loss in Huntington's disease. *Brain* 138: 3327–44.

13. Poudel GR, Stout JC, Domínguez D JF, Churchyard A, Chua P, Egan GF, Georgiou-Karistianis N (2015): Longitudinal change in white matter microstructure in Huntington's disease: The IMAGE-HD study. *Neurobiol Dis* 74: 406–12.

14. Tabrizi SJ, Reilmann R, Roos R, Durr A, Leavitt B, Owen G, *et al.* (2012): Potential endpoints for clinical trials in premanifest and early Huntington's disease in the TRACK-HD study: analysis of 24 month observational data. *Lancet Neurol* 11: 42–53.

15. Hobbs NZ, Henley SMD, Ridgway GR, Wild EJ, Barker RA, Scahill RI, *et al.* (2010): The progression of regional atrophy in premanifest and early Huntington's disease: a longitudinal voxel-based morphometry study. *J Neurol Neurosurg Psychiatry* 81: 756–763.

16. Aylward EH, Nopoulos PC, Ross CA, Langbehn DR, Pierson RK, Mills JA, *et al.* (2011): Longitudinal change in regional brain volumes in prodromal Huntington disease. *J Neurol Neurosurg Psychiatry* 82: 405–410.

17. Rosas HD, Salat DH, Lee SY, Zaleta AK, Pappu V, Fischl B, *et al.* (2008): Cerebral cortex and the clinical expression of Huntington's disease: complexity and heterogeneity. *Brain*

131: 1057–1068.

18. Estrada-Sánchez AM, Rebec G V. (2013): Role of cerebral cortex in the neuropathology of Huntington's disease. *Front Neural Circuits* 7. https://doi.org/10.3389/fncir.2013.00019

19. Ramirez□Garcia G, Galvez V, Diaz R, Bayliss L, Fernandez□Ruiz J, Campos□Romo A (2019): Longitudinal atrophy characterization of cortical and subcortical gray matter in Huntington's disease patients. *Eur J Neurosci* ejn.14617.

20. Mehrabi NF, Waldvogel HJ, Tippett LJ, Hogg VM, Synek BJ, Faull RLM (2016): Symptom heterogeneity in Huntington's disease correlates with neuronal degeneration in the cerebral cortex. *Neurobiol Dis* 96: 67–74.

21. Tabrizi SJ, Leavitt BR, Landwehrmeyer GB, Wild EJ, Saft C, Barker RA, *et al.* (2019): Targeting Huntingtin Expression in Patients with Huntington's Disease. *N Engl J Med* NEJMoa1900907.

22. Friston KJ, Litvak V, Oswal A, Razi A, Stephan KE, Van Wijk BCM, *et al.* (2016): Bayesian model reduction and empirical Bayes for group (DCM) studies. *Neuroimage* 128: 413–431.

23. Ziegler G, Ridgway GR, Blakemore S-J, Ashburner J, Penny W (2017): Multivariate dynamical modelling of structural change during development. *Neuroimage* 147: 746–762.

24. Friston KJ, Mattout J, Trujillo-Barreto N, Ashburner J, Penny W (2007): Variational free energy and the Laplace approximation. *Neuroimage* 34: 220–234.

25. Klöppel S, Gregory S, Scheller E, Minkova L, Razi A, Durr A, *et al.* (2015): Compensation in Preclinical Huntington's Disease: Evidence From the Track-On HD Study. *EBioMedicine* 2: 1420–9.

26. Ho A, Hocaoglu M (2011): Impact of Huntington's across the entire disease spectrum: The phases and stages of disease from the patient perspective. *Clin Genet*. https://doi.org/10.1111/j.1399-0004.2011.01748.x

27. Johnson EB, Gregory S, Johnson HJ, Durr A, Leavitt BR, Roos RA, *et al.* (2017): Recommendations for the use of automated gray matter segmentation tools: Evidence from Huntington's disease. *Front Neurol* 8. https://doi.org/10.3389/fneur.2017.00519

28. Hobbs NZ, Barnes J, Frost C, Henley SMD, Wild EJ, Macdonald K, *et al.* (2010): Onset and

progression of pathologic atrophy in Huntington disease: A longitudinal MR imaging study. *Am J Neuroradiol* 31: 1036–1041.

29. Huntington Study Group (1996): Unified Huntington's Disease Rating Scale: reliability and consistency. *Mov Disord* 11: 136–42.

30. Smith A (1991): *Symbol Digit Modalities Test*. Los Angeles: Western Psychological Services.

31. Paulsen JS, Smith MM, Long JD (2013): Cognitive decline in prodromal Huntington disease: Implications for clinical trials. *J Neurol Neurosurg Psychiatry*. https://doi.org/10.1136/jnnp-2013-305114

32. Stout JC, Jones R, Labuschagne I, O'Regan AM, Say MJ, Dumas EM, *et al.* (2012): Evaluation of longitudinal 12 and 24 month cognitive outcomes in premanifest and early Huntington's disease. *J Neurol Neurosurg Psychiatry*. https://doi.org/10.1136/jnnp-2011-301940

33. Ashburner J, Ridgway GR (2012): Symmetric diffeomorphic modeling of longitudinal structural MRI. *Front Neurosci* 6: 197.

34. Ledig C, Heckemann RA, Hammers A, Lopez JC, Newcombe VFJ, Makropoulos A, *et al.* (2015): Robust whole-brain segmentation: application to traumatic brain injury. *Med Image Anal* 21: 40–58.

35. Gelman A (2006): Multilevel (hierarchical) modeling: What It can and cannot do. *Technometrics*. https://doi.org/10.1198/004017005000000661

36. Zeidman P, Jafarian A, Seghier ML, Litvak V, Cagnan H, Price CJ, Friston KJ (2019): A guide to group effective connectivity analysis, part 2: Second level analysis with PEB. *Neuroimage*. https://doi.org/10.1016/j.neuroimage.2019.06.032

37. Zeidman P, Jafarian A, Corbin N, Seghier ML, Razi A, Price CJ, Friston KJ (2019): A guide to group effective connectivity analysis, part 1: First level analysis with DCM for fMRI. *Neuroimage*. https://doi.org/10.1016/j.neuroimage.2019.06.031

38. Jack CR, Knopman DS, Jagust WJ, Shaw LM, Aisen PS, Weiner MW, *et al.* (2010): Hypothetical model of dynamic biomarkers of the Alzheimer's pathological cascade. *The Lancet Neurology*. https://doi.org/10.1016/S1474-4422(09)70299-6

39. Lorenzi M, Filippone M, Frisoni GB, Alexander DC, Ourselin S (2019): Probabilistic disease progression modeling to characterize diagnostic uncertainty: Application to staging and prediction in Alzheimer's disease. *NeuroImage*. https://doi.org/10.1016/j.neuroimage.2017.08.059

40. Oxtoby NP, Young AL, Cash DM, Benzinger TLS, Fagan AM, Morris JC, *et al.* (2018): Data-driven models of dominantly-inherited Alzheimer's disease progression. *Brain*. https://doi.org/10.1093/brain/awy050

41. Oxtoby NP, Alexander DC (2017): Imaging plus X: Multimodal models of neurodegenerative disease. *Current Opinion in Neurology*. https://doi.org/10.1097/WCO.0000000000000460

42. Penny WD (2012): Comparing dynamic causal models using AIC, BIC and free energy. *Neuroimage* 59: 319–330.

43. Wasserstein RL, Lazar NA (2016): The ASA's Statement on p-Values: Context, Process, and Purpose. *Am Stat* 70: 129–133.

44. Group HS (1996): Unified Huntington's Disease Rating Scale: reliability and consistency. Huntington Study Group. *Mov Disord* 11: 136–142.

45. Aylward EH, Anderson NB, Bylsma FW, Wagster M V., Barta PE, Sherr M, *et al.* (1998): Frontal lobe volume in patients with Huntington's disease. *Neurology* 50: 252–258.

46. Halliday G, McRitchie DA, Macdonald V, Double KL, Trent RJ, McCusker EA (1998): Regional Specificity of Brain Atrophy in Huntington's Disease. *Exp Neurol* 154: 663–672.

47. Duff K, Paulsen JS, Beglinger LJ, Langbehn DR, Wang C, Stout JC, *et al.* (2010): "Frontal" Behaviors Before the Diagnosis of Huntington's Disease and Their Relationship to Markers of Disease Progression: Evidence of Early Lack of Awareness. *J Neuropsychiatry Clin Neurosci*. https://doi.org/10.1176/jnp.2010.22.2.196

48. Scahill RI, Hobbs NZ, Say MJ, Bechtel N, Henley SMD, Hyare H, *et al.* (2013): Clinical impairment in premanifest and early Huntington's disease is associated with regionally specific atrophy. *Hum Brain Mapp* 34: 519–529.

49. Silva PHR, Spedo CT, Baldassarini CR, Benini CD, Ferreira DA, Barreira AA, Leoni RF (2019): Brain functional and effective connectivity underlying the information processing

speed assessed by the Symbol Digit Modalities Test. *Neuroimage*. https://doi.org/10.1016/j.neuroimage.2018.09.080

50. Silva PHR, Spedo CT, Barreira AA, Leoni RF (2018): Symbol Digit Modalities Test adaptation for Magnetic Resonance Imaging environment: A systematic review and meta-analysis. *Multiple Sclerosis and Related Disorders*. https://doi.org/10.1016/j.msard.2018.01.014

51. Rosenblatt A, Kumar B V., Mo A, Welsh CS, Margolis RL, Ross CA (2012): Age, CAG repeat length, and clinical progression in Huntington's disease. *Mov Disord* 27: 272–276.

52. Ruocco HH, Bonilha L, Li LM, Lopes-Cendes I, Cendes F, Kramer B, *et al.* (2008): Longitudinal analysis of regional grey matter loss in Huntington disease: Effects of the length of the expanded CAG repeat. *J Neurol Neurosurg Psychiatry* 79: 130–135.

53. Henley SM, Wild EJ, Hobbs NZ, Scahill RI, Ridgway GR, MacManus DG, *et al.* (2009): Relationship between CAG repeat length and brain volume in premanifest and early Huntington's disease. *J Neurol* 256: 203–212.

54. Coppen EM, van der Grond J, Hafkemeijer A, Rombouts SARB, Roos RAC (2016): Early grey matter changes in structural covariance networks in Huntington's disease. *NeuroImage Clin* 12: 806–814.

55. Cash DM, Bocchetta M, Thomas DL, Dick KM, van Swieten JC, Borroni B, *et al.* (2018): Patterns of gray matter atrophy in genetic frontotemporal dementia: results from the GENFI study. *Neurobiol Aging*. https://doi.org/10.1016/j.neurobiolaging.2017.10.008

56. Cash DM, Frost C, Iheme LO, Ünay D, Kandemir M, Fripp J, *et al.* (2015): Assessing atrophy measurement techniques in dementia: Results from the MIRIAD atrophy challenge. *Neuroimage* 123: 149–164.

57. Willett JB (1989): Some Results on Reliability for the Longitudinal Measurement of Change: Implications for the Design of Studies of Individual Growth. *Educ Psychol Meas* 49: 587–602.

Author contributions:

TRACK-HD Investigators designed the experiment. E.J., G.Z., S.G., R.S. and W.P. conducted the experiment and analyzed the data. E.J., G.Z., and S.G. wrote the paper. G.R. edited the manuscript. S.T. was Principal Investigator of the TRACK-HD and TrackOn-HD studies, and edited the manuscript.

Acknowledgments and funding:

The authors wish to thank the TRACK-HD and TrackOn-HD study participants and the CHDI Foundation, a not-for-profit organization dedicating to finding treatments for HD. Some of this work was undertaken at University College London Hospital/University College London, which received funding from the Department of Health NIHR Biomedical Research Centres funding scheme. EBJ, SJT, RIS and SG are supported by a Wellcome Trust Collaborative Award (grant code 200181/Z/15/Z). GZ would like to thank Emrah Düzel for support at the DZNE.

This paper has been shared as a preprint on bioRxiv, with the DOI https://doi.org/10.1101/537977.

TRACK-HD Investigators:

AUSTRALIA Monash University, Victoria: SC Andrews, JC Campbell, M Campbell, E Frajman A O'Regan, I Labuschagne, C Milchman, C Pourchot, S Queller, JC Stout; CANADA University of British Columbia, Vancouver: A Coleman, R Dar Santos, J Decolongon, B Leavitt, A Sturrock FRANCE APHP, Hôpital Salpêtriere, Paris: E Bardinet, A Durr, C Jauffret, D Justo, S Lehericy, C Marelli, K Nigaud, R Valabrègue; GERMANY University of Münster, Münster: N Bechtel, S Bohlen, R Reilmann; University of Bochum, Bochum: A Hoffman, P Kraus; University of Ulm, Ulm: GB Landwehrmeyer. NETHERLANDS Leiden University Medical Centre, Leiden: SJA van den Bogaard, EM Dumas, J van der Grond, EP t'Hart, C Jurgens, RAC Roos, M-N Witjes-Ane. U.K. St Mary's Hospital, Manchester: N Arran, J Callaghan, D Craufurd, C Stopford; London School of Hygiene and Tropical Medicine, London: C Frost, R Jones; University College London, London: H Crawford, NC Fox, C Gibbard, NZ Hobbs, N Lahiri, I Malone, R Ordidge, G Owen, A Patel, T Pepple, J Read, MJ Say, E Wild, D

Whitehead; Imperial College London, London: S Keenan; IXICO, London: D M Cash; University of Oxford, Oxford: C Berna, S Hicks, C Kennard. U.S.A. University of Iowa, Iowa City, IA: T Acharya, E Axelson, H Johnson, DR Langbehn, C Wang; Massachusetts General Hospital, Harvard, MA: S Lee, W Monaco, HD Rosas; Indiana University, IN: C Campbell, S Queller, K Whitlock; CHDI Foundation, New York, NY: B Borowsky, AJ Tobin.

TrackOn-HD investigators:

AUSTRALIA Monash University, Victoria: SC Andrews, I Labuschagne, JC Stout. CANADA University of British Columbia, Vancouver: J Decolongon, M Fan, T Koren, T Petkau, B Leavitt; FRANCE ICM and APHP, Hôpital Salpêtriere, Paris: A Durr, C Jauffret, D Justo, S Lehericy, K Nigaud, R Valabrègue; GERMANY Freiburg University, Freiburg: S Kloppel, L Mincova, Scheller E; George Huntington Institute, Munster: R Reilmann, N Weber; University of Ulm, Ulm: B Landwehrmeyer, I Mayer, M Orth; NETHERLANDS Leiden University Medical Centre, Leiden: SJA van den Bogaard, RAC Roos, EP ‘t Hart, A Schoonderbeek; U.K. London School of Hygiene and Tropical Medicine, London: A Cassidy, C Frost, R Keogh; Manchester University, Manchester: D Craufurd; University College London, London: C Berna, H Crawford, M Desikan, R Ghosh, D Hensman, EB Johnson, D Mahaleskshmi, I Malone, P McColgan, M Papoutsi, J Read, A Razi, G Owen; U.S.A. University of Iowa, Iowa City, IA: H Johnson, DR Langbehn, Long J, Mills, J. CHDI Foundation, New York, NY: B Borowsky.

Competing interest:

All authors report no biomedical financial interests or potential conflicts of interest.

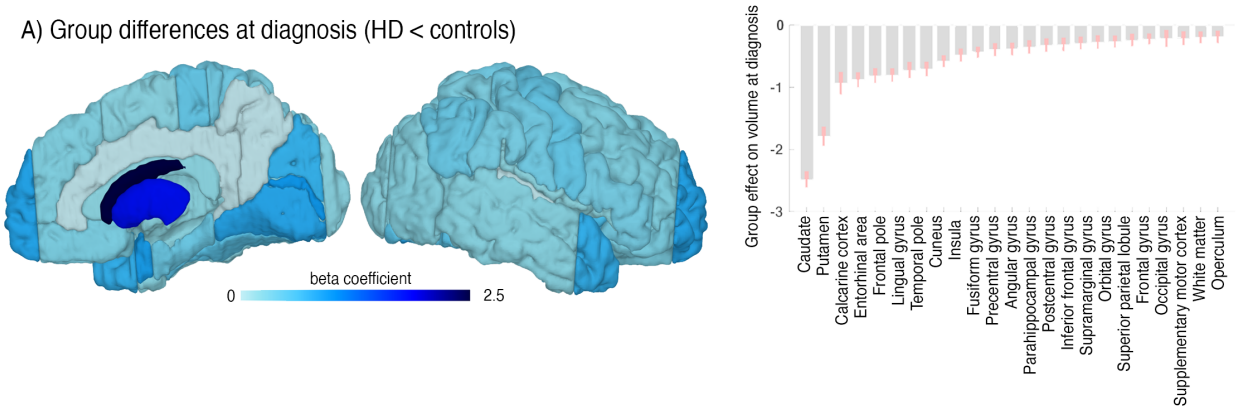

A) Total volume loss in all regions for HD and control participants

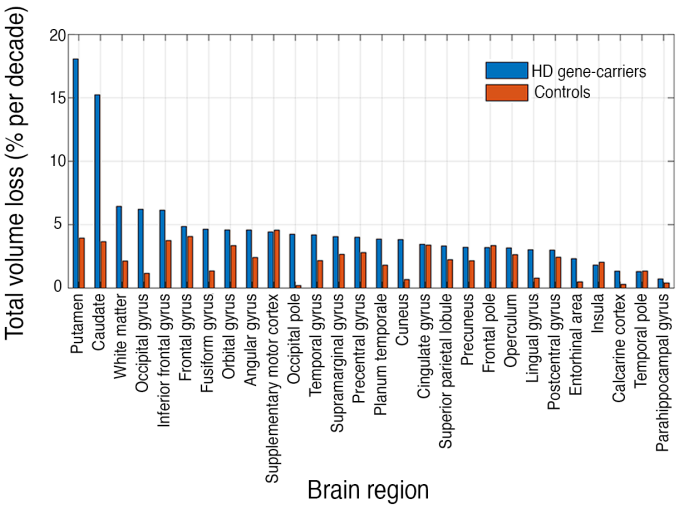

B) Group differences in rate of rate of atrophy (decay; HD > controls)

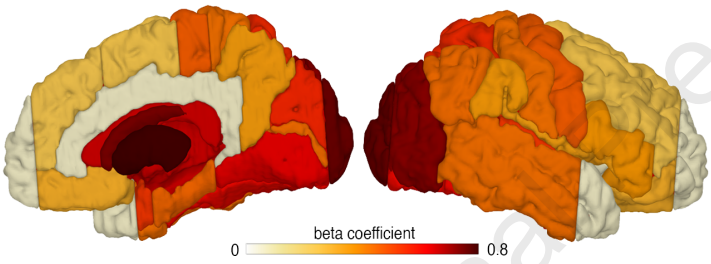

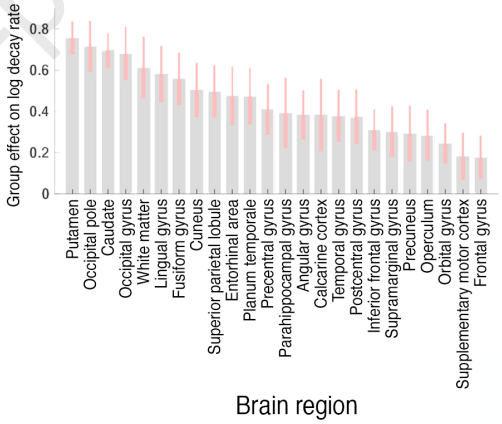

A) Higher CAG length increases rate of atrophy (decay)

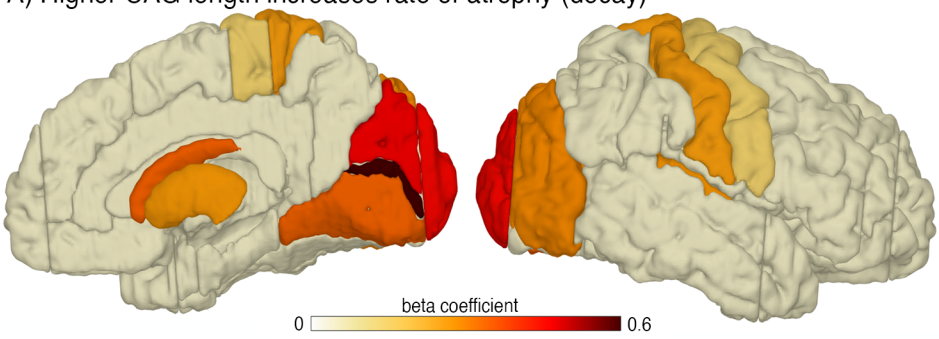

B)

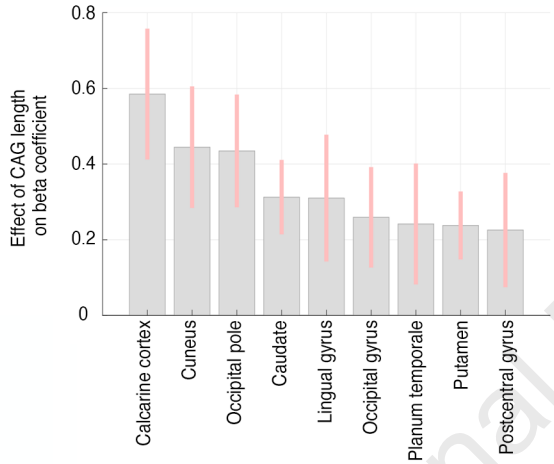

C)

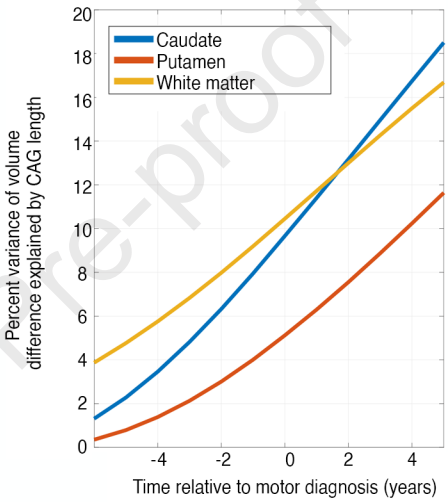

A) Atrophy in brain regions that contributes to worsening Total Motor Score (TMS)

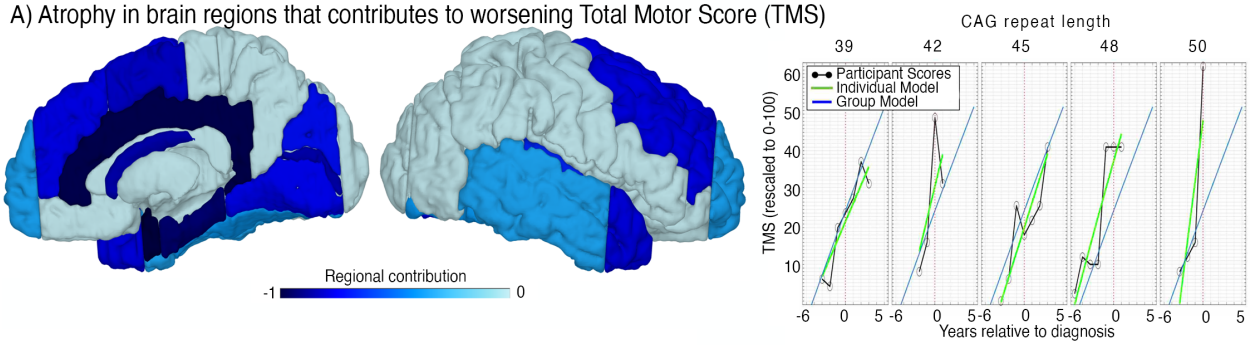

B) Atrophy in brain regions that contributes to worsening Symbol Digit Modalities Test (SDMT)